Spectrally resolved ion imaging from laser produced plasmas using CR-39 detectors

Cite as: AIP Advances **11**, 015232 (2021); https://doi.org/10.1063/5.0031930
Submitted: 07 October 2020 • Accepted: 19 November 2020 • Published Online: 12 January 2021

S. V. Rahul, Rakesh Y. Kumar, T. Sairam, et al.

Spectrally resolved ion imaging from laser produced plasmas using CR-39 detectors

Cite as: AIP Advances 11, 015232 (2021); doi: 10.1063/5.0031930
Submitted: 7 October 2020 • Accepted: 19 November 2020 •
Published Online: 12 January 2021

S. V. Rahul,[1] Rakesh Y. Kumar,[1,2] T. Sairam,[1] Ratul Sabui,[1,2] Angana Mondal,[3] V. Rakesh Kumar,[3] Amit D. Lad,[3] Yash M. Ved,[3] Kedar Mal,[4] R. Gopal,[1] and M. Krishnamurthy[1,3,a)]

AFFILIATIONS

[1]TIFR Hyderabad, 36/P, Gopanpally Village, Serilingampally Mandal, Ranga Reddy District, Hyderabad 500107, India
[2]Indian Institute of Technology Hyderabad, Kandi 502285, India
[3]Tata Institute of Fundamental Research, Homi Bhabha Road, Colaba, Mumbai 400005, India
[4]Inter-University Accelerator Centre, Aruna Asaf Ali Marg, Near Vasant Kunj, New Delhi 110067, India

[a)]**Author to whom correspondence should be addressed:** mkrism@tifr.res.in

ABSTRACT

Intense laser-produced plasmas generate bright, ultrashort bursts of accelerated ions. Reducing the required laser intensity and increasing the repetition rate of the laser to generate high energy ions is important, and mesoscopic particle targets are an attractive option to address this issue. Newer experimental strategies to measure ion energies and their angular distribution are needed in studies of such systems. In this paper, we outline a method to simultaneously measure these quantities using a single CR39 film. Although CR-39 detectors are known for ion imaging or spectroscopy, combining these specially for lower ion energies and applications to low-intensity laser experiments is not common. The paradigm chosen in our study is to consider the spatial distribution of nuclear tracks on a CR-39 sheet, while simultaneously separating them by their track diameter. Our method achieves an energy resolution of about 100 keV and a spatial resolution of tens of micrometers. In addition, ion species other than protons, i.e., carbon and oxygen, can also be imaged in an energy-resolved manner.

I. INTRODUCTION

Intense laser pulses have been used to create hot, dense plasmas with relativistic electron temperatures. These hot plasmas have shown strong promise as table-top sources of accelerated ions[1,2] and neutral atoms[3,4] with energies of several million electron volts. Depending on the laser and target parameters, various acceleration mechanisms might be possible. For relativistic intensity lasers interacting with foil targets with micrometer thickness, ions from hydrocarbon impurity layers on targets may be accelerated by the TNSA process to energies of several million electron volts.[5–7] Similarly, energetic ions may also be produced from isolated, nanometer sized gas cluster targets[4,8–10] via mechanisms like a Coulomb explosion. The angular distribution of the accelerated ions can be very different among different processes.

Mesoscopic mass limited targets present an important size intermediate between these two length scales of targetry. Mass limited solid density targets of several micrometers size, in the form of microdroplets[11–15] or aerosol jets,[16,17] can be routinely generated. Their capability to be generated at high repetition rates and to generate hotter plasmas[15,18,19] makes them attractive to use with laser pulses of moderate intensity. Studies of laser plasma interactions using such lasers aim to develop high brightness and low-emittance secondary sources of electrons, x-rays, and ions. Whereas such lasers may not be intense enough to generate multi-million electron volt ions, their capability to generate compact, high brightness, ultrashort bursts of lower energy ions (<500 keV) at high repetition rates, nevertheless, makes them interesting.

However, such high repetition rate targetry in conjunction with low attainable ion energies presents a novel set of challenges for ion diagnosis. Evaporation of the liquid or the background gases in the aerosol puff may contribute to poor chamber vacuum (0.1 mbar –1 mbar). In addition, significant particulate debris may be present from the aerosol particles as well. The mean stopping range of the ions is also reduced at higher chamber pressures, requiring compact diagnostics.

Complementary ion diagnostics are often employed in laser plasma experiments. Ion spectrometers like Thomson parabola spectrometers may be used for measuring the ion spectrum with high resolution, by sampling ions through a small aperture.[20–22] Ion emission over larger solid angles may be probed using imaging detectors which allow the measurement of angular distribution, source size, and transverse beam emittance. Micro-Channel Plates (MCPs),[11] Radiochromic Films (RCFs)[23] and Solid State Nuclear Track Detectors (SSNTDs)[24] are typically employed for this purpose. Methods capable of simultaneously imaging ions, while resolving ion energy, are of tremendous importance.[23] Indeed, such diagnostics are critical to applications such as time resolved point-projection radiography using ions accelerated from laser produced plasmas.[25,26]

In the context of high repetition rate experiments, the use of MCPs is severely constrained by the chamber vacuum conditions and the presence of strong EMP bursts generated in intense laser–solid interaction.[27,28] RCF stacks, relying on the position of the Bragg peak of the ions stopping in a particular layer, can be used for energy resolved imaging of proton beams of several million electron volts. However, for the energy ranges considered above, all the ions can be stopped either in the first layer of the stack or, especially for heavy ions, in the protective layer of the RCF. Hence, methods to simultaneously diagnose the ion spatial and spectral distributions in this energy window represent an important contemporary lacuna, which has remained unexplored.

CR-39 has been extensively employed in the past for passive detection of ions and neutral particles. It is sensitive to single particle hits, and it is highly selective, being insensitive to energetic electrons, x-rays, and EMPs. Extracting quantitative information from CR-39 films involves etching in a hot alkaline solution, microscopic imaging of the etched detector, and counting the number density of nuclear tracks left by ion impact.

The utility of CR39 toward ion spectrometry has been demonstrated using temporal growth rates of nuclear tracks[29] in multi-step etching or, simply, track diameters[30–32] in a single etching step, as a metric. However, the limited field of view of the microscopic objectives implies that only small solid angles can be sampled this way. Using CR-39 for ion imaging relies on counting track number densities across the irradiated region.[16,24] Not much attention has been paid to simultaneously considering their track diameters.

Generating spectrally resolved ion images from CR-39 detectors requires solving multiple issues. Essentially, we require simultaneous measurement of diameters and the number densities of nuclear tracks. This requires seamlessly imaging large areas (several cm^2) of CR-39 with high fidelity and microscopic spatial resolution. The resultant images might be much larger than the available memory on workstations readily available. They also need to be efficiently processed within the time scales of an experimental campaign, in order to be useful. Furthermore, etching conditions need to be carefully selected to ensure a good spectral resolution and dynamic range.

The premise of our report is to outline a methodology to use nuclear track detectors for reconstructing energy resolved ion images. Using an ion accelerator and previous calibrations,[30] we measure the change in the track diameter with energy for ion species of relevance to our experiments. The calibrated track diameters are then used to obtain the energy resolved images of ions of all species and not just protons. We show a simple working demonstration of the method using traces from a Thomson parabola spectrometer. Furthermore, we show how the method may be applied to experiments involving intense laser generating plasmas from mesoscopic particles and outline the difficulties involved in the process. Our method is very general and relies on imaging large regions (several mm^2 to cm^2) of CR39 with micrometer resolution. Thus, we obtain ion images with good resolution, both in energy and space. The ability to do this at close proximity of the laser plasma without ion traversal is very advantageous for ion studies in poor vacuum conditions.

II. CR-39 PROCESSING

A. Etching

The relationship of energy (E_i) and track diameter (D_t) is central for ascertaining the spectrum. Such a calibration curve needs to be monotonic over the range of ion energies considered and sets the dynamic attainable energy range of the spectrometry. Additionally, given the optical imaging resolution, the value dD_t/dE_i is directly correlated with the spectral resolution and is desired to be large. These are the two factors that influenced our choice of etching conditions.

In this context, we followed the etching conditions given in Ref. 30. Their experiments demonstrated that proton track diameters increase monotonically until 1 MeV, with dD_t/dE_i values of 2.5 μm/100 keV. Then, the track diameters decrease again monotonically, for energies larger than 1 MeV. In the interest of extension to higher energy ranges in the future, apart from suitability to our energy range, we chose these conditions.

CR-39 sheets of size 5 cm × 5 cm having a thickness of 200 μm, supplied by Track Analysis Systems Ltd., were used throughout all the experiments. After irradiation with the ions, CR-39 pieces are etched in a bath of 6.25 N NaOH placed in a temperature controlled oil bath at 90 °C for a duration of 4 h, following the etching method in Ref. 30. The etched sheets are then thoroughly rinsed with DI water and allowed to dry on a bed of soft paper tissue, and they are subsequently mounted on the slides for microscopic examination.

B. Image acquisition

Tracks on CR-39 must be characterized with respect to their position and diameter to extract quantitative information on ion emission. This means scanning large regions (about 5 cm × 5 cm) with a resolution enough to resolve the diameter of the tracks for a practical experiment in imaging proton beams. The imaging then demands solution to a two-fold problem: (a) imaging a large sample region with microscopic resolution without the loss of focus and (b) to stitch the images seamlessly.

We address these problems by employing a commercial microscopy system (Olympus IX83, running the CellSens software). We use a 20× infinity corrected objective with a numerical aperture of 0.4. The images are captured by a CCD Camera (Retiga 6000 Monochrome) with a square pixel size of 4.54 μm × 4.54 μm. Hence, every pixel in the acquired raw images corresponds to a spatial distance of 0.23 μm. This is sampling rate with which the spatial distance is sampled. The true spatial imaging resolution of

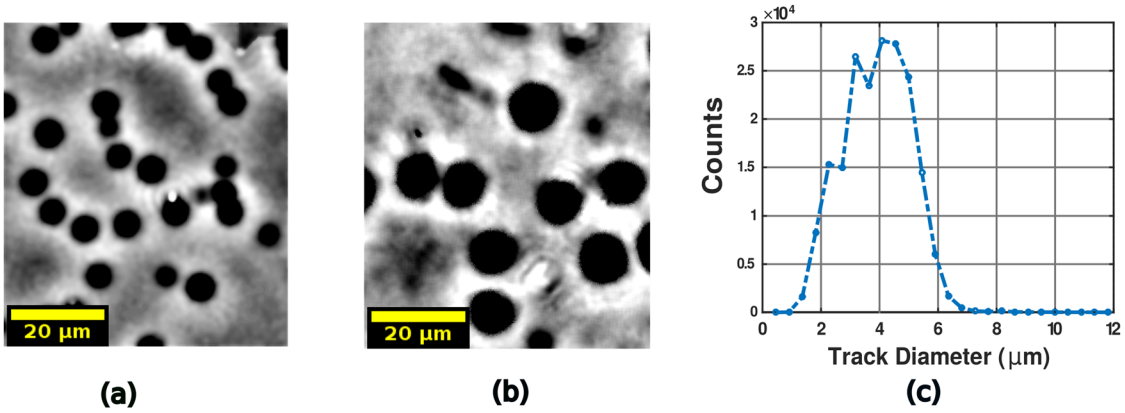

FIG. 1. Representative images of pits formed upon etching CR-39 after exposure to different ion species and ion energies: (a) 200 keV C^+ and (b) 350 keV O^+ and (c) representative track diameter distribution for 100 keV C^+ ions. The track diameter is measured across all the tracks, and a histogram of the track diameters is presented above. This histogram is subsequently fitted with a Gaussian distribution to yield the track diameter distributions summarized in Table I. The track diameter can be used to spatially resolve ion emission of a given energy.

the microscope, however, is governed by the diffraction limit of the microscope and is calculated to be about 0.9 μm. This combination allows for well sampled measurement of nuclear tracks with diameters greater than a few micrometers, as observed in our experiments. We scanned the samples in the phase contrast imaging mode. Typical images of the obtained tracks are given in Fig. 1.

The microscopic system allows mounting of the detector sheets on an automated micro-positioning stage. The detector is then rastered across the field of view of the microscopic objective as individual images are acquired by the controlling computer and stitched together. While imaging large spatial regions with microscopic resolution, it is essential to keep the object being imaged within the focal plane of the objective. For the microscopic objective used here, the depth of field was about 5 μm. In practice, the object can be off-focus by larger values. Buckling of thin films of CR39 while mounting and differential ion doses were found to be the major contributors to this issue.

Hence, a compensation method was necessary to keep the detector surface being imaged in focus. Our acquisition software allows sampling of the planes of the best focus on selected points across the object, prior to the actual imaging routine. These points can then be used to calculate the approximate surface morphology of the surface focal plane across the sample. This reconstructed "focal map" was then employed by the acquisition software to position the sample within the focal plane of the microscopic objective. If the focal plane can be sampled over a sufficient number of points over the CR-39 surface, this focal map is sufficiently satisfactory and allows the entire size of the detector sheet to be seamlessly imaged.

C. Image processing

Figure 1 shows a magnified picture of the ion tracks formed when CR-39 is exposed to ions of different species and energy from an accelerator. The tracks on CR-39 as seen with a microscope are circular in nature. Hence, the problem of spectrally separating the incident ions reduces to the detection of the position and radii of all the circles on the image. We use the circle detection routines in MATLAB, based on circular Hough transform algorithms to detect the position and diameter of the circles on the images.

The image sub-sections are fed into the computer memory. A top-hat filter corrects non-uniform illumination in the microscopic images. The Hough transform procedure is sensitive to the presence of noise in the system, and hence, a Wiener filter is employed to filter noise. These images are segmented using an Otsu thresholding method. These binary images are then used for circle detection using circular Hough transform libraries of MATLAB.[33] Using this, we obtain a list of positions and the corresponding radii of the detected circles. This list is subsequently sorted by their radii. For every radius value, the list of center values is further binned together in bins of size 100 pixels × 100 pixels, to yield a two dimensional spatial histogram. This yields the spectrally and spatially resolved ion yields of ion flux incident on the detector. Hence, for a given track radius, the spatial bin gives the "pixel" position of the ion yield and vertical axis given in the false color of the image, indicating the counts of nuclear tracks registered in the bin.

Depending on the area being imaged, the microscopic images of CR-39 can be fairly large. For CR39 sheets of dimensions considered above, the resulting images were up to 200 000 pixels × 200 000 pixels in dimension and 80 GB–100 GB in size. As such, it was not always possible to process them with the memory available (used 8 GB–16 GB) on a desktop workstation. Hence, the images are split into sub-sections, each of which is independently processed on a separate core of the workstation using a Linux tool GNU parallel.[34] The detected circle positions and radii across all sections can then be collated together and processed.

III. EXPERIMENTAL CALIBRATION OF TRACK DIAMETERS USING AN ECR ION SOURCE

For the CR-39 detectors to be used for ion imaging, their dependence on nuclear track diameters must be characterized for ion energies for the species of relevance. Track diameter calibrations in the multi-million electron volt ion energy ranges have been well explored in the past.[30,35,36] For protons, calibration data ranges over

a very wide spectral range also exist.[30–32,37–39] However, the calibration measurements for heavier ions in the ion range 100 keV –350 keV is sparse even in these experiments. For ranges of ion energies (<350 keV), to the best of our knowledge, the relationship of the track diameters to ion energies is not well established. Hence, in this section, we measure the track diameter vs energy relation for carbon and oxygen ions in the energy window of 100 keV–350 kilo-electron volts.

A. Experimental details

This calibration run was performed using the ions produced from a 10 GHz Nanogan type ECR ion source stationed at the IUAC, New Delhi, which can provide a wide range of energies from a few tens of kilo-electron volts to a few million electron volts.[40] The nuclear track detectors used in our experiment operate in the single particle counting mode, which would mean an ion current of less than 100 fA per sq.mm. However, the ECR accelerator is designed to deliver ion currents greater than several microamperes. Hence, we require a method to bring down the flux of ions incident on the detector to within a single particle regime.

The ion beam is swept across a 1 cm aperture in the collector which collects electrons from the target irradiated with the ion beam. The flux of ions is initially diagnosed using a scintillator coupled with a camera, and the current is gradually brought down until the scintillation is barely visible. The beam is next incident on a Faraday cup coupled to the electrometer, where the current of the charged particles is measured. The beam position is swept across the hole in the collector. The sweeping parameters are tuned until the current on the electrometer reads a few picoamperes, which is its least count. The objective was only to reduce the ion flux sufficiently to obtain non-overlapping tracks. Hence, rather than systematically measuring the beam current vs ion beam sweeping parameters, the operation was optimized empirically in a few trials. Nearly 10^5 clearly resolved tracks could be easily obtained in a 1 cm^2 region.

B. Results

Table I summarizes the ion species used in this calibration and their respective mean track diameters, calculated using the above-mentioned method. In principle, under our experimental conditions, obtaining calibrations for higher energies would mandatorily require higher charge species in this system. Since a convolution of calibration with the charge states is not advisable, we limit our calibrations to 350 keV. However, a monotonic behavior in the calibration curve of the track diameter and energy has been previously observed in multiple studies.[31,35,36] Consequently, procedures similar to the ones outlined below can be applied for higher energy ranges once a monotonic relationship between ion energy and the track diameter has been established.

Despite ensuring the lowest possible current using this method, we found that the middle of the beam splat image of the aperture on CR-39 may be saturated, especially for higher energy ions. However, individual scattered ion tracks can still be observed away from the center of the splat. Measuring the track diameter distribution, across this unsaturated region, then, gives the distribution of track diameters for the given ion energy, as seen in the representative images of the ion tracks in Fig. 1.

The resultant track diameter distribution, for C^+ ions with an energy of 100 keV, for instance, is illustrated in Fig. 1(c). This track diameter distribution is fitted with a single component Gaussian function, and the resultant calculated standard deviation is used for calculating the error bars over the mean track diameter. The results of the track diameter calibration are summarized in Table I. It can clearly be observed that the average track diameters increase monotonically with the increase in input ion beam energy for a given ion species. Even with the observed energy resolution, application of this method to intense laser plasma studies is advantageous as shown below. We find that error due to the measurement of the track diameter is much smaller than the statistical variation in the track diameter seen for a given ion energy. The energy resolution is therefore limited by the intrinsic ion matter interaction in this system.

This energy resolution may be further improved based on the etching conditions, as detailed in Sec. II. Usually, short etching times are generally more preferable. However, an increase in the etching time, given the etching temperature and etchant concentrations, can result in increasing the slope of the track diameter v/s energy curve.[30,36,37] This should improve the spectral resolution of the detector. Increasing the temperature of the etch bath[30] can significantly reduce the time taken to reach high track diameters.

The limit on the attainable spatial resolution is set by the bin size in the 2-D histogram of track counts, which itself has a lower limit of the diameter of the nuclear track. Hence, increasing track diameters to improve spectral resolution comes at the cost of a reduced spatial resolution. This property of CR39 represents a limitation in the attainable resolutions. Nevertheless, the parameter space of the etching conditions should be fully explored in order to decide the optimal balance between spatial and spectral resolution to conduct a spectral imaging measurement with CR39.

TABLE I. Track Diameters and fitted standard deviations for O^+ and C^+ ions.

Species	Energy (keV)	Track diameter (μm)
O^+	100	4 ± 2.1
O^+	200	5 ± 1.5
O^+	350	8 ± 2.0
C^+	100	4 ± 1.8
C^+	200	6 ± 0.9
C^+	350	11 ± 1.4

IV. THOMSON PARABOLA

To further establish the technique, we demonstrate the ability of using the track diameter spatial distributions with a standard Thomson parabola spectrometer. To understand the constituents of the ions emitted from the front of the target, Thomson parabola (TP) spectrometer diagnostics have been extensively employed in the past by various groups. In this spectrometer, a combination of parallel electric and magnetic fields is used to separate ions sampled through an aperture, by their charge-to-mass ratio. Ions of a given mass to charge ratio form a parabola. The intensity distribution along the parabola is used to retrieve the energy spectrum. This allows for an

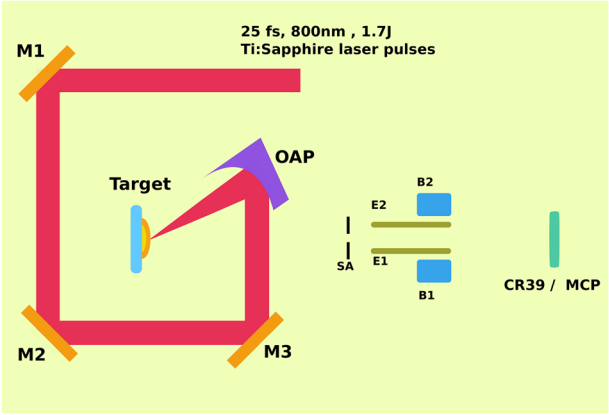

FIG. 2. Schematic of the Thomson parabola spectrometer: M1, M2, M3, and M4 are the guiding mirrors in the chamber for the input laser beam. The laser has a center wavelength of 800 nm, with a pulse duration of 25 fs, and 1.7 J/pulse. This is focused using an off-axis parabola (OAP) of a focal length of 250 mm on an aluminum coated BK7 glass slab (target). E1 and E2 and B1 and B2 are the electric and magnetic field plates, respectively, in the spectrometer. SA is a 100 μm sampling aperture. An MCP or CR-39 is used as the detector screen for backward accelerated ions.

attractive route to performing additional calibration of track diameters for the energy range in question. We obtain a unique mapping for the track diameters to the energy, as required for our technique. Unlike different experimental runs with different ion energies, the laser plasma experiments exhibit advantages such as simultaneous measurement of wide ion energy and the ability to evaluate intrinsic energy resolution with the CR-39 detector.

A. Experimental setup

We use a Thomson parabola spectrometer having an MCP coupled to a phosphor scintillator screen, described previously in Ref. 20. This was designed to diagnose the ion that accelerated from solid density plasmas produced by a 150 TW class laser. The ion signal was initially optimized on the. Subsequently, the MCP was replaced with a CR-39 sheet to detect ion parabola traces. The experiments were carried out with a 150 TW class Ti:sapphire laser stationed at TIFR, Mumbai, and the experimental schematic is illustrated in Fig. 2. The laser delivered pulses with a 25 fs duration at a 10 Hz repetition rate with a center wavelength of 800 nm. Each pulse carries about 1.7 J of energy and is focused using an off-axis parabola mirror with a focal length of 250 mm to a focal spot size (FWHM) of 10 μm, resulting in a focused intensity of 2.1×10^{19} W/cm^{-2}.

Ions and neutrals enter the TP chamber through a 100 μm aperture. The experimental schematic is given in Fig. 2. An aluminum coated BK-7 glass is used as the solid target. The spectrometer is operated with an electric field of 50 V/cm and a magnetic field of 150 G. An MCP with 40 mm diameter or CR-39 sheets of size 5 cm $\times$ 5 cm and 200 μm thickness are replaceably used as detectors.

B. Results

Figure 3 illustrates comparative images and the proton spectrum obtained from MCP and CR39. All points in spectra (b) and (d) are proportional to the ion count (N) and hence contain a counting error of $\sqrt{N}$ owing to Poisonnian statistics.

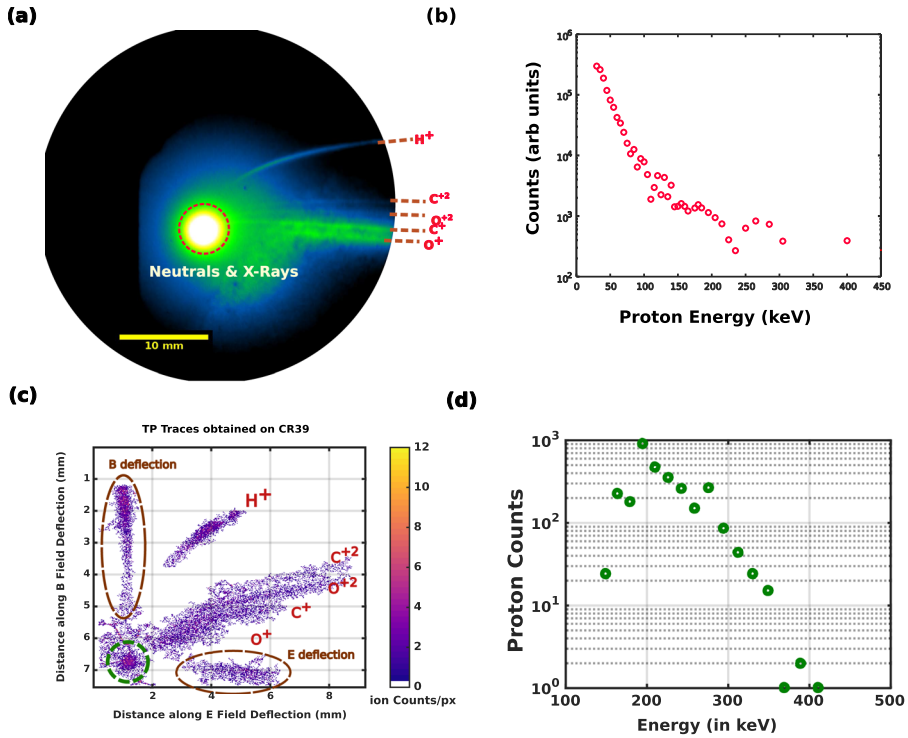

FIG. 3. Comparison of Thomson parabola traces observed on the (a) MCP and (c) CR-39. The red circle in (c) and the circle in (a) indicate the neutral atom spot. The parabolae corresponding to the various ionic species (H^+, C^{+q}, and O^{+q} for q = 1 and 2) are illustrated. The colorbar in (c) illustrates the total ion counts on every pixel of the image. In addition, the trace corresponding to the E and B field deflection is also illustrated. The respective proton spectra extracted from the images are illustrated in (b) and (d).

Representative Thomson parabola traces observed on the MCP are shown in Fig. 3(a). In addition to the accelerated protons, multiple charged states of heavier ions, viz., carbon and oxygen, are also visible. The proton spectrum extracted from this trace is given in Fig. 3(b). The central spot in this case is largely due to neutral atoms from the plasma along with some scattering light, x-rays.[20] The central spot can interfere with the high energy end of the spectrum and make the cut-off energy measurement difficult. The cutoff energy measurement is, however, is not limited as adequate voltages are used to well separate the high energy ions from the central spot.

Figure 3(c) shows a map of Thomson parabola track density observed on the CR-39 detector using the methodology described above. We also collected traces with either only magnetic field or electric field applied in the TP. This gives us a direct marker for both the dispersion axes and is important to extract ion energies from the TP traces. Such an exercise is also performed with the MCP. Since the MCP is an online detector, traces with only B or E fields are collected separately, and only the trace with both the fields is shown. Since the analysis of CR-39 is only possible offline, we take all the three runs—with only the E-field, with only the B-field, and both simultaneously—on the same detector sheet. The color bar alongside illustrates the number of ion tracks observed per pixel and is obtained by binning the number of tracks in the original image in a two dimensional histogram with a bin area of 100 × 100 pixels. Each pixel value corresponds to the number of tracks in a 22 μm × 22 μm area. Hence, this process of binning sets the spatial resolution. As such, this value can be chosen according to the diameter of the largest track observed in the experiment. The image shown is from multiple shots, with the laser incident on a fresh portion of the target each time.

This TP trace is integrated over all track diameters. The spectrum of protons is extracted as shown in Fig. 3(d) by using the spectral imaging method. This is obtained by creating an image mask around the proton trace for all the frames, to only filter the proton trace. By counting the track number in every frame, and converting the proton track diameter to energy using the calibration described in Ref. 30, the proton spectrum can be obtained. From Fig. 3(d), it can be observed that the maximum energy of the protons obtained from CR-39 detectors is about 350 keV.

We note that TP images and the data extracted from the two may appear different due to the differences in the methodology described below, but the salient features of the measurements are, however, consistent. The MCP is used here in the current mode and handles a large range of ion flux. The detector is about 40 mm and has no low energy detection threshold in the ion energy regime of kilo-electron volt–million electron volt. Since the ion energy is determined by the position on the detector, the energy scale is continuous. The low energy cutoff happens only by the ion dispersion out of the large detector. The dynamic range of ion detection is over a few orders of magnitude. CR-39, on the other hand, has a much larger low energy cut-off and is set by the etching conditions (about 150 keV in the present experiment). The ion detection is by particle count, and the ion spectrum is obtained by binning the track diameters. The energy resolution is set by the track diameter measurement, apart from the intrinsic deviations in the track diameter.

For the current operating conditions, only ions below 50 keV are deflected off the detector in the MCP images. Low energy ion (50 keV–100 keV) emission is with two orders of magnitude larger flux. Due to the signal collection with the large flux, the MCP ion image appears sharper in the low energy part of the spectrum. In the higher energy range, the parabolae interfere with the large signal in the center. The dominant signal at the center is due a large fraction[3] of neutral atoms of C and O that are below 100 keV. Pulsing the MCP bias voltage can be used to remove the ion signal due to the neutral atoms, leading to an improvement in the signal-to-noise ratio. In this experiment, we, however, did not use the gating technique as we wanted to simultaneously measure the energy spectrum of the heavier ions. Track formation in CR-39 is highly sensitive to ions and neutral atoms and is insensitive to electromagnetic radiation. In our experimental conditions, we have not noticed visible ion tracks for energies below 150 keV. Hence, it can be readily observed that the size of the central spot, and the noise in its vicinity, is significantly smaller in the case of CR39 shots (<1 mm approx.) than that observed for the MCP (5 mm approx). Indeed, spatially separated parabolae can be seen in the region of CR39 images, where the MCP still shows a saturated central spot.

To ensure that the measurement with both methods are consistent, we bin the ion energy spectrum obtained with the MCP detector in the same conditions as per the limitations of CR-39 which has a poorer energy resolution. Figure 4 shows the result of such a comparison. As seen, the ion energy spectrum detected by both methods compares well. The proton temperatures in both the cases are similar (91 keV and 92 keV), and the maximum proton energy measured is the same. CR-39 has limitations in the energy resolution. However, it is important to note that the two parameters, ion temperature and maximum ion energy, that are vital to laser plasma studies are measured equally well with CR-39. The added advantage of getting a spatial image of the ion emission and the possibility of extracting spectrally gated distribution without any necessity for an electric or magnetic field dispersion at the close proximity of the laser focus are important to the laser plasma studies.

By filtering the images by the track diameter, spectrally resolved images of the Thomson parabola traces can be obtained. This is

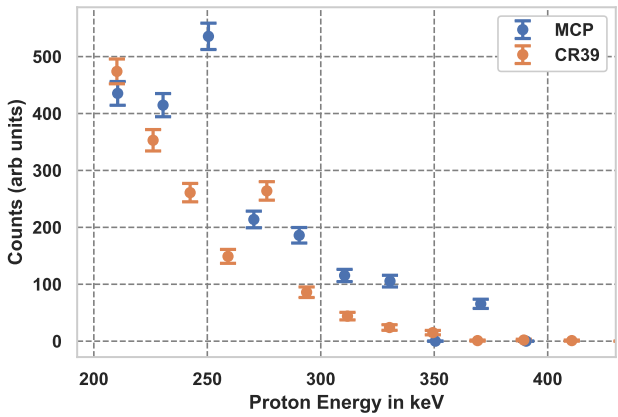

FIG. 4. Comparison of the ion spectra measured with the MCP and CR-39 in the spectral range from 200 to 400 keV. The MCP ion spectrum shown in Fig. 3(b) is binned with the same parameters as that used in CR-39. The ion temperature and the maximum ion energy are measured well with CR-39 despite the poorer energy resolution.

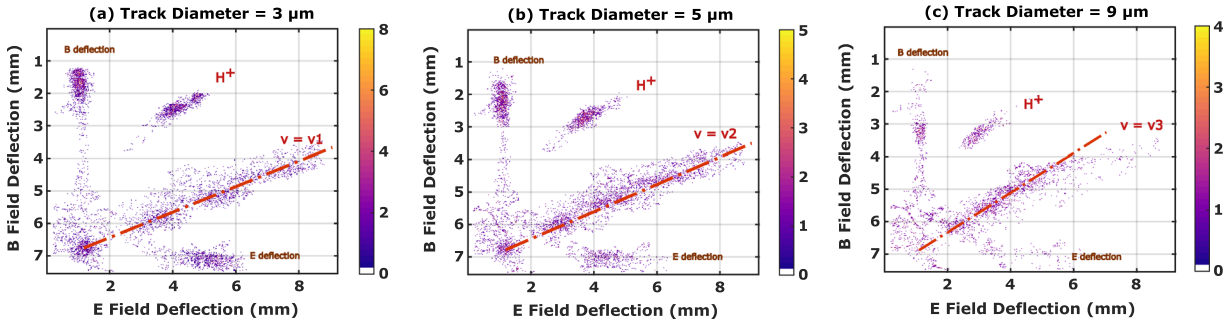

FIG. 5. Spectrally resolved images of Thomson parabola traces on CR-39 for average track diameters of (a) 3 μm, (b) 5 μm, and (c) 9 μm corresponding to mean proton energies of (a) 190 keV, (b) 230 keV, and (c) 290 keV. The colorbar indicates the number of ion tracks. For protons, the parabola sections progressively approach closer to the origin as the track diameter is increased. For carbon and oxygen ions, additionally, the lines of constant velocity, passing through the origin, progressively increase in the slope when the track diameter is increased.

illustrated in Fig. 5. In a Thomson parabola trace, the ions with the lowest energies get the maximum deflection in the spectrometer fields. Hence, these are the ions which are farther from the central spot. Along the parabola, the ion energies are higher for points closer to the central spot. The diameter of the nuclear tracks for ions also increases monotonically with energy. Sections of proton traces with a difference in mean energy of about 100 keV have a track diameter sufficiently different to be clearly seen separately in these image sequences. This can be seen in Figs. 5(a) and 5(c), where parts of proton traces of mean energies of about 190 keV and 290 keV can be observed. This allows us to infer that the present technique has a spectral resolution of about 100 keV for protons. Previous calibrations[30] indicate that the proton track diameters should increase monotonically until about 1 MeV, allowing our technique to work well until 1 MeV.

In addition, the sub-sections of parabolae corresponding to charge states of carbon and oxygen can also be seen clearly. It is important to observe that nuclear tracks across different species having approximately the same track diameter lie on a common straight line. In context of the Thomson parabola traces, this is the line of a constant velocity, with the slope of the line defining the velocity of the ions. It can also be readily observed that the slope of this straight line increases systematically as tracks of higher diameters are observed.

This leads us to infer three facts applicable to the energy range of our observations of a few hundred kilo-electron volts for carbon and oxygen. First, this indicates that for a given charge state of an ion, the track diameter increases monotonically with an increase in energy. Second, the track diameter does not seem to depend on the charge state of the ion in question. Finally, between ions of different elements, for instance, carbon and oxygen, this would imply a dependence of the track diameter on the velocity of the accelerated ions in question, rather than on their energies.

V. EXPERIMENTAL TEST OF SPECTRAL IMAGING USING MICRODROPLET ACCELERATED IONS

Mesoscopic mass limited particles are attractive targets to generate hot plasmas. They may be delivered to the interaction region as isolated microparticles in Paul traps[14,41] or in aerosol jets,[16,17] they may be mounted on support,[42] or they may be delivered as microdroplet streams.[11–13,15,18,43] Here, we study the acceleration of ions due to the interaction of microparticulate targets from an aerosol source with high repetition rate, moderate intensity laser pulses. The details of the experimental apparatus used to generate such a source are outlined in Ref. 17. The authors in that paper demonstrated the use of such targets as a high repetition rate x-ray source generating x-ray bremsstrahlung with energies up to about 100 keV. Here, we outline a utility of our track diameter resolved imaging method to understand the ion acceleration mechanisms at play during such an interaction.

A. Experimental setup

Figure 6(a) illustrates the experimental schematic employed to measure the angular distribution of ions ejected from the microdroplet–laser interaction. The experiment was carried out using 25 fs, 2 mJ laser pulses from a Ti:sapphire laser operating at a repetition rate of 1 kHz.

An aerosol puff of boric acid microparticles was constantly supplied to the target chamber using the method described in Ref. 17. In brief, pressurized nitrogen gas was passed through a bed of particles, which were constantly agitated in a separate chamber connected to the main vacuum chamber. A small fraction of the particles get picked up by the gas and are carried with it to the interaction region in the main vacuum chamber. The mean size of the particles was measured to be 14μm. Typically, only 10% of the particles are hit by the intense laser pulses and converted to plasma. The chamber pressure was held at 1 mbar, with the carrier gas used in the experiment being the contributor to the low vacuum.

CR-39 sheets 5 cm × 5 cm in size and 200 μm thick were installed in one quadrant of the vacuum chamber, to diagnose the angular distribution of ions. The distance of CR39 from the target was 3.6 cm. CR-39 was exposed to the ion source for a total time of 150 s, accumulating a total of 15 000 shots (considering a 10% interaction probability, as above). They are taken out of the vacuum chamber. Etching, image acquisition, and processing were carried out as explained in the previous sections. Figure 6(b) shows the ion

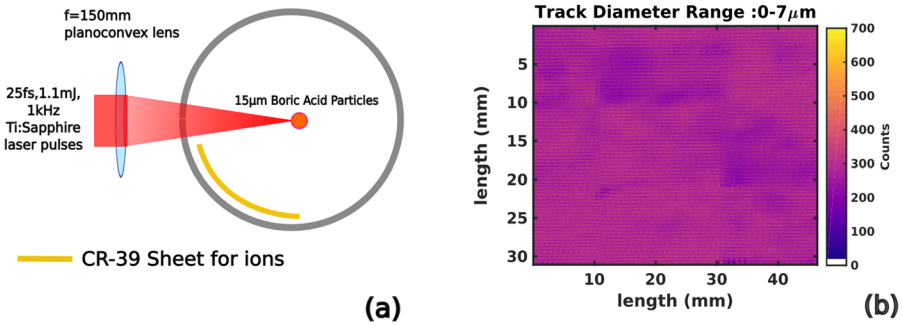

FIG. 6. (a) Schematic of the experiment to measure the angular distribution of accelerated ions from a microparticulate target. (b) A false color picture of the ions impinged on the CR-39 film giving a nuclear track < 7μm. The color indicates a near uniform yield of the ions along the length and breadth of the CR-39 film, indicating an isotropic distribution.

image extracted from CR-39. The color indicates the ion yield at any given position. In this image, only the ions with track diameters <7 μm, corresponding only to the first peak of the ion energy spectrum, are included.

B. Results

Figure 7(a) illustrates the track diameter distribution spectrum. The arrows indicate the ion energy. It can be observed that the distribution has a bimodal character. A low energy ion peak and a high energy ion peak extend up to about 500 keV. We conjecture that this distribution might simply imply two different acceleration mechanisms at play.

Looking at track diameter resolved ion intensity maps indeed leads credence to this conjecture. Figure 7(b) gives the ion angular distributions extracted for each of the two peaks of the ion spectrum. We observe that for the ions corresponding to ions of track diameters lesser than 7 μm, the entire CR-39 sheet has a uniform distribution of ion counts [see Fig. 6(b)]. It leads us to infer that these ions of lower energy, < 250 keV for protons and < 200 keV for carbon and oxygen, are isotropically distributed. Interestingly, for ions of larger track diameters, i.e., from 7 μm to 14 μm, we observe a very different distribution. These ions may be seen to be emitted anisotropically.

Such features of ion beams emanating from spherical microtargets have been reported before in the literature. Previous studies[16] on the interaction of such microdroplets indicate that the curved nature of such droplets might encourage a strong resonance absorption at angles away from the laser propagation direction. This encourages hot electron production and, subsequently, directional proton emission. Furthermore, their experimental and simulations also suggest the isotropic expansion of the low energy component of proton emission.

It is important to note that conventional track counting, without simultaneously considering their radii, will not differentiate the isotropic and anisotropic part contributions of the ion emission. From Fig. 6(b), we note that the typical counts of the high energy anisotropic ions are nearly an order of magnitude smaller than that for the higher energy species. Hence, an anisotropic nature of the beam would be difficult to conclusively establish from track density alone. Similarly, using CR-39 as proton spectrometers limits the details of their directional emission. By simultaneously measuring both spatial and spectral distribution of the nuclear tracks, it is possible to correctly deconvolve the contributions due to different features of ion emission.

For the boric acid microparticulate targets used here, various ionic species may be accelerated, viz., H^+, C^{q+}, B^{q+}, and O^{q+}. The dominant accelerated species is strongly dependent on the relative pre-plasma density scale lengths. Since the only parameter of the tracks considered in our report is the diameter of the tracks, the nature of ion species incident on the detector is not deciphered in this measurement. This might require, for instance, the use of a conventional Thomson parabola spectrometer to provide high resolution energy spectra of different species. The contribution of protons, compared to the heavier ions of C^{q+} and O^{q+}, can also be simply inferred using thin absorber foils which only transmit protons, while completely stopping heavier ions. In this article, however, we have focused on the properties of angular distributions of ions, and we intend to use this diagnostic for future research.

We note that we can indeed extract the ion spectrum from these measurements. Comprehending the physics of the acceleration, the distribution of ion species, and the ion energy spectra generated for

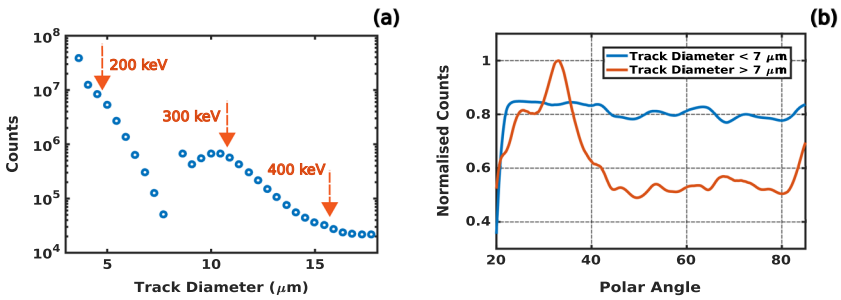

FIG. 7. (a) Ion yields as a function of the track diameter extracted from the CR-39 film image. The arrows indicate the ion energy. The ion energy spectrum has two dominant energy components. (b) Angular distribution of the ions in the two peaks shown in (a). Low energy ions with a smaller track diameter are isotropic while the high energy ions show quasi-beam like emission at about 30° to the laser incidence.

these laser intensities is beyond the scope of this paper. The present report is primarily to establish a proof of principle of the ion spectral imaging method. Systematic experiments and calculations detailing the complete physics of the ion acceleration from such targets and the angular distribution for higher energy ions will be outlined in a future report.

VI. CONCLUSIONS AND FUTURE WORK

In conclusion, we have demonstrated imaging of laser accelerated ions using CR-39 detectors in an energy resolved manner. This spectral imaging technique can image protons with a spectral resolution of about 100 keV. This is about an order of magnitude improvement in the proton spectral resolution as compared to results of previous methods based on RCF stack imaging.[23] Furthermore, the spatial imaging resolution in this case is defined by the size of binning used to produce ion intensity maps of ion spatial distribution. In our experiments, a spatial resolution of a few tens of microns was attainable.

In addition, our technique is not limited to imaging protons alone, unlike the previous demonstrations of the RCF stack imaging technique. Given a complete calibration of track diameters of ions accelerated in a particular experiment, spectrally resolved ion imaging can be undertaken for any ion or neutral atom species.

The core of our technique relies on circle detection in large microscopic image sets of CR-39. Our experiments were undertaken as a proof of principle using commercial microscopy systems, and the circle detection was performed on a multi-core workstation. However, significant speedup in the computational times of image processing can be obtained using, for example, graphical processing units (GPUs), which are specialized for this application. Similarly, dedicated systems for fast analysis of microscopic images of CR-39 over large systems have also been reported previously.[44] These systems can also dramatically bring down the microscopic imaging time for CR-39 detectors. The present technique might find its use in ion radiography and, importantly, in the diagnosis of angular distribution and emittance of laser produced ion beams.

ACKNOWLEDGMENTS

We thank the DAE for all financial support for the experiments. The advice of Dr. C. P. Safvan and Dr. Pragya Bhatt from the IUAC for beam tuning methods on the ECR ion source at the IUAC is gratefully acknowledged. We wish to thank members of Dr. Aprotim Mazumdar's and Dr. T. N. Narayanan's laboratory in the TIFR for their help with the microscopy and the chemistry lab facility. We thank P. P. Rajeev for his help in many stages of this work. M.K. also acknowledges the DAE-SRC-OI grant.

DATA AVAILABILITY

The data that support the findings of this study are available from the corresponding author upon reasonable request.

REFERENCES

[1] A. Macchi, M. Borghesi, and M. Passoni, Rev. Mod. Phys. **85**, 751 (2013).
[2] H. Daido, M. Nishiuchi, and A. S. Pirozhkov, Rep. Prog. Phys. **75**, 056401 (2012).
[3] S. Tata, A. Mondal, S. Sarkar, J. Jha, Y. Ved, A. D. Lad, J. Colgan, J. Pasley, and M. Krishnamurthy, Phys. Rev. Lett. **121**, 134801 (2018).
[4] R. Rajeev, T. Madhu Trivikram, K. P. M. Rishad, V. Narayanan, E. Krishnakumar, and M. Krishnamurthy, Nat. Phys. **9**, 185 (2013).
[5] M. Hegelich, S. Karsch, G. Pretzler, D. Habs, K. Witte, W. Guenther, M. Allen, A. Blazevic, J. Fuchs, J. Gauthier *et al.*, Phys. Rev. Lett. **89**, 085002 (2002).
[6] A. Maksimchuk, S. Gu, K. Flippo, D. Umstadter, and V. Y. Bychenkov, Phys. Rev. Lett. **84**, 4108 (2000).
[7] E. L. Clark, K. Krushelnick, J. R. Davies, M. Zepf, M. Tatarakis, F. N. Beg, A. Machacek, P. A. Norreys, M. I. K. Santala, I. Watts *et al.*, Phys. Rev. Lett. **84**, 670 (2000).
[8] T. Ditmire, J. W. G. Tisch, E. Springate, M. B. Mason, N. Hay, J. P. Marangos, and M. H. R. Hutchinson, Phys. Rev. Lett. **78**, 2732 (1997).
[9] T. Ditmire, J. W. G. Tisch, E. Springate, M. B. Mason, N. Hay, R. A. Smith, J. Marangos, and M. H. R. Hutchinson, Nature **386**, 54 (1997).
[10] V. Kumarappan, M. Krishnamurthy, and D. Mathur, Phys. Rev. Lett. **87**, 085005 (2001).
[11] T. Sokollik, M. Schnürer, S. Steinke, P. Nickles, W. Sandner, M. Amin, T. Toncian, O. Willi, and A. Andreev, Phys. Rev. Lett. **103**, 135003 (2009).
[12] S. Ter-Avetisyan, M. Schnürer, S. Busch, E. Risse, P. Nickles, and W. Sandner, Phys. Rev. Lett. **93**, 155006 (2004).
[13] S. Ter-Avetisyan, M. Schnürer, P. Nickles, M. Kalashnikov, E. Risse, T. Sokollik, W. Sandner, A. Andreev, and V. Tikhonchuk, Phys. Rev. Lett. **96**, 145006 (2006).
[14] T. Sokollik, T. Paasch-Colberg, K. Gorling, U. Eichmann, M. Schnürer, S. Steinke, P. V. Nickles, A. Andreev, and W. Sandner, New J. Phys. **12**, 113013 (2010).
[15] M. Anand, S. Kahaly, G. Ravindra Kumar, M. Krishnamurthy, A. S. Sandhu, and P. Gibbon, Appl. Phys. Lett. **88**, 181111 (2006).
[16] X.-Y. Peng, J. Zhang, J. Zheng, Z.-M. Sheng, M.-H. Xu, Z.-Y. Zheng, T.-J. Liang, Y.-T. Li, Q.-L. Dong, X.-H. Yuan, Y.-J. Li, and H.-M. Li, Phys. Rev. E **74**, 036405 (2006).
[17] R. Gopal, R. Kumar, M. Anand, A. Kulkarni, D. P. Singh, S. R. Krishnan, V. Sharma, and M. Krishnamurthy, Rev. Sci. Instrum. **88**, 023301 (2017).
[18] M. Anand, P. Gibbon, and M. Krishnamurthy, Europhys. Lett. **80**, 25002 (2007).
[19] J. T. Morrison, E. A. Chowdhury, K. D. Frische, S. Feister, V. M. Ovchinnikov, J. A. Nees, C. Orban, R. R. Freeman, and W. M. Roquemore, Phys. Plasmas **22**, 043101 (2015).
[20] S. Tata, A. Mondal, S. Sarkar, A. D. Lad, and M. Krishnamurthy, Rev. Sci. Instrum. **88**, 083305 (2017).
[21] R. Rajeev, K. P. M. Rishad, T. M. Trivikram, V. Narayanan, and M. Krishnamurthy, Rev. Sci. Instrum. **82**, 083303 (2011).
[22] K. Harres, M. Schollmeier, E. Brambrink, P. Audebert, A. Blažević, K. Flippo, D. C. Gautier, M. Geißel, B. M. Hegelich, F. Nürnberg *et al.*, Rev. Sci. Instrum. **79**, 093306 (2008).
[23] F. Nürnberg, M. Schollmeier, E. Brambrink, A. Blažević, D. C. Carroll, K. Flippo, D. C. Gautier, M. Geißel, K. Harres, B. M. Hegelich *et al.*, Rev. Sci. Instrum. **80**, 033301 (2009).
[24] F. Lindau, O. Lundh, A. Persson, P. McKenna, K. Osvay, D. Batani, and C.-G. Wahlström, Phys. Rev. Lett. **95**, 175002 (2005).
[25] M. Borghesi, A. Schiavi, D. H. Campbell, M. G. Haines, O. Willi, A. J. Mackinnon, P. Patel, M. Galimberti, and L. A. Gizzi, Rev. Sci. Instrum. **74**, 1688 (2003).
[26] S. Kar, H. Ahmed, R. Prasad, M. Cerchez, S. Brauckmann, B. Aurand, G. Cantono, P. Hadjisolomou, C. L. Lewis, A. Macchi *et al.*, Nat. Commun. **7**, 10792 (2016).
[27] M. J. Mead, D. Neely, J. Gauoin, R. Heathcote, and P. Patel, Rev. Sci. Instrum. **75**, 4225 (2004).
[28] C. Stoeckl, V. Y. Glebov, P. A. Jaanimagi, J. P. Knauer, D. D. Meyerhofer, T. C. Sangster, M. Storm, S. Sublett, W. Theobald, M. H. Key *et al.*, Rev. Sci. Instrum. **77**, 10F506 (2006).
[29] F. Bahrami, F. Mianji, R. Faghihi, M. Taheri, and A. Ansarinejad, Nucl. Instrum. Methods Phys. Res., Sect. A **813**, 96 (2016).
[30] M. Seimetz, P. Bellido, P. García, P. Mur, A. Iborra, A. Soriano, T. Hülber, J. García López, M. C. Jiménez-Ramos, R. Lera *et al.*, Rev. Sci. Instrum. **89**, 023302 (2018).

[31] A. Szydłowski, M. Sadowski, T. Czyżewski, M. Jaskóła, and A. Korman, Nucl. Instrum. Methods Phys. Res., Sect. B **149**, 113 (1999).
[32] C. Baccou, V. Yahia, S. Depierreux, C. Neuville, C. Goyon, F. Consoli, R. De Angelis, J. E. Ducret, G. Boutoux, J. Rafelski *et al.*, Rev. Sci. Instrum. **86**, 083307 (2015).
[33] H. Yuen, J. Princen, J. Illingworth, and J. Kittler, Image Vision Comput. **8**, 71 (1990).
[34] O. Tange *et al.*, USENIX Mag. **36**, 42 (2011).
[35] T. W. Jeong, P. Singh, C. Scullion, H. Ahmed, P. Hadjisolomou, C. Jeon, H. Yun, K. Kakolee, M. Borghesi, and S. Ter-Avetisyan, Sci. Rep. **7**, 2152 (2017).
[36] V. Romo, J. Rickards, G. Espinosa, and J. I. Golzarri, Radiat. Prot. Dosim. **85**, 459 (1999).
[37] A. Malinowska, A. Szydłowski, M. Jaskóła, A. Korman, B. Sartowska, T. Kuehn, and M. Kuk, Rev. Sci. Instrum. **84**, 073511 (2013).
[38] J. Y. Lee, J. H. Jo, S. H. Park, K. Lee, Y. W. Lee, K.-H. Yea, Y. H. Cha, and Y. U. Jeong, J. Korean Phys. Soc. **51**, 426 (2007).
[39] D. Xiaojiao, L. Xiaofei, T. Zhixin, H. Yongsheng, G. Shilun, Y. Dawei, and W. Naiyan, Nucl. Instrum. Methods Phys. Res., Sect. A **609**, 190 (2009).
[40] G. Rodrigues, K. Mal, N. Kumar, R. Baskaran, P. Lakshmy, Y. Mathur, P. Kumar, D. Kanjilal, and A. Roy, Rev. Sci. Instrum. **85**, 02A944 (2014).
[41] T. M. Ostermayr, D. Haffa, P. Hilz, V. Pauw, K. Allinger, K.-U. Bamberg, P. Böhl, C. Bömer, P. Bolton, F. Deutschmann *et al.*, Phys. Rev. E **94**, 033208 (2016).
[42] A. Henig, D. Kiefer, M. Geissler, S. G. Rykovanov, R. Ramis, R. Hörlein, J. Osterhoff, Z. Major, L. Veisz, S. Karsch *et al.*, Phys. Rev. Lett. **102**, 095002 (2009).
[43] J. Hah, G. M. Petrov, J. A. Nees, Z.-H. He, M. D. Hammig, K. Krushelnick, and A. G. R. Thomas, Appl. Phys. Lett. **109**, 144102 (2016).
[44] N. Yasuda, K. Namiki, Y. Honma, Y. Umeshima, Y. Marumo, H. Ishii, and E. Benton, Radiat. Meas. **40**, 311 (2005).